Article

Simple, Large-Scale Fabrication of Uniform Raman-Enhancing Substrate with Enhancement Saturation

Daejong Yang, Hyunjun Cho, Sukmo Koo, Sagar R Vaidyanathan, Kelly Woo, Youngzoon Yoon, and Hyuck Choo

ACS Appl. Mater. Interfaces, **Just Accepted Manuscript** • Publication Date (Web): 28 Apr 2017

Simple, Large-Scale Fabrication of Uniform Raman-Enhancing Substrate with Enhancement Saturation

Daejong Yang[1], Hyunjun Cho[2], Sukmo Koo[1], Sagar R. Vaidyanathan[2], Kelly Woo[2], Youngzoon Yoon[3], and Hyuck Choo[1,2,]*

[1] Department of Medical Engineering, California Institute of Technology, Pasadena, CA 91125, United States

[2] Department of Electrical Engineering, California Institute of Technology, Pasadena, CA 91125, United States

[3] Device Lab, Device & System Research Center, Samsung Advanced Institute of Technology (SAIT), Suwon, 16678, Republic of Korea

KEYWORDS

surface enhanced Raman scattering, three-dimensional nanostructure, gold nanoparticle, biosensor, large scale,

ABSTRACT

It is well known that gold nanoparticle (AuNP) clusters generate strong surface-enhanced Raman scattering (SERS). In order to produce spatially uniform Raman-enhancing substrates at a large

scale, we synthesized vertically perforated three-dimensional (3D) AuNP stacks. The 3D stacks were fabricated by first hydrothermally synthesizing ZnO nanowires perpendicular to silicon wafers followed by repetitively performing liquid-phase deposition of AuNPs on the tops and side surfaces of the nanowires. During the deposition process, the nanowires were shown to gradually dissolve away, leaving hollow vestiges or perforations surrounded by stacks of AuNPs. Simulation studies and experimental measurements reveal these nanoscale perforations serve as light paths that allow the excitation light to excite deeper regions of the 3D stacks for stronger overall Raman emission. Combined with properly sized nanoparticles, this feature maximizes and saturates the Raman enhancement at 1-pM sensitivity across the entire wafer-scale substrate, and the saturation improves the wafer-scale uniformity by a factor of six when compared to nanoparticle layers deposited directly on a silicon wafer substrate. Using the 3D-stacked substrates, quantitative sensing of adenine molecules yielded concentrations measurements within 10% of the known value. Understanding the enhancing mechanisms and engineering the 3D stacks have opened a new method of harnessing the intense SERS observed in nanoparticle clusters and realize practical SERS substrates with significantly improved uniformity suitable for quantitative chemical sensing.

INTRODUCTION

Surface-enhanced Raman scattering (SERS) spectroscopy has great potential for chemical and biological sensing due to its high sensitivity and selectivity obtained through relatively simple optical measurements.[1] Due to these advantages, SERS has been widely studied since M. Fleischmann et al.[2] first observed the phenomenon in 1974 and researchers have

continuously attempted to understand the underlying enhancement mechanisms in order to develop commercially viable SERS products.[3]

The mechanisms of SERS are still under investigation and are predicted to originate from electromagnetic effects and chemical interactions.[4-7] Electromagnetic enhancement effects are believed to be the dominant enhancing mechanism for SERS and are generated when laser irradiation excite plasmons on the surfaces of the noble metals structures that form the substrate, creating hot spots at nanoscale tips and gaps.[7-8] Chemical enhancement is attributed to electrochemical interactions between analyte molecules and the metal atoms of the substrate.[6, 9-11]

Effective SERS substrates are typically obtained by randomly roughening 2 dimensional (2D) metal films or coating the substrate with metal nanoparticles.[12-13] More elaborate 3-dimensional (3D) structures providing larger effective hot spot areas, such as stacked nanoparticles and pyramids, have been shown to increase adsorption of target molecules and further enhance Raman emission intensities.[14-19] Researchers have recently favored simpler fabrication methods by implementing nanowires made of ZnO,[14-15] TiO_2,[16] Si,[17] Cu_2O,[18] and NiO[19], which allow flexibility regarding to nanoscale sizes and shapes of the 3D SERS substrates.

For practical applications, spatial uniformity of Raman enhancement is as important as the magnitude of SERS intensity. It is essential for making scientifically useful and commercially viable SERS substrates for quantitative sensing. Some researchers have attempted to address the uniformity issue by engineering nanoscale optical antennas using top-down fabrication processes, however the substrates have failed to produce strong, spatially uniform SERS.[20] Incomplete understanding of the mechanism of SERS combined with fabrication

challenges controlling the positions, sizes, and shapes of nanoscale structures on a large substrate, such as a silicon wafer, have made it difficult to set proper engineering goals for realizing strong, spatially uniform SERS substrates.[21-23]

Here we report 3D stacked gold nanoparticle (AuNP) SERS substrates with improved spatial uniformity. Instead of relying on 2D nanoscale patterned structures such as optical antenna, nanoparticle clusters were utilized for their strong Raman enhancing properties. A dense ZnO nanowire array (Figure 1A) was synthesized on a Si wafer substrate, serving as a framework for 3D deposition of AuNP stacks and improve nanoparticle distribution. Next liquid phase deposition (LPD) of AuNPs was performed, resulting in 10-20 nm diameter nanoparticles attached on the tops and side walls of the nanowires (Figure 1A).[24] After multiple LPD repetitions, the AuNPs became efficiently stacked and the nanowires gradually dissolved leaving hollow vestiges or perforations behind. These perforated light paths not only generate effective inter-particle gaps for enhancement, but also allow the excitation light to reach deeper into the stack and promote the otherwise hidden nanoparticle layers to participate in Raman enhancement. Their presence assures the number of nanoparticle layers participating in Raman enhancement is nearly constant across the entire substrate as long as the nanoparticle layer is sufficiently thick,[25] which generates uniformly saturated Raman enhancement across on the entire substrate. As such, the wafer-scale, uniform Raman enhancement of this approach has proven to be highly tolerant of variations in the final geometries of the stacks. Experimental measurements were confirmed by a series of finite-difference time-domain (FDTD) simulations, and quantitative sensing of nano-molar to micro-molar adenine solutions were demonstrated within 10% accuracy.

RESULTS AND DISCUSSION

Fabrication

The fabrication of 3D stacked ZnO nanowire-based AuNP substrates (3DNP-X where X is the number of LPD repetitions) consists of two successive processes: hydrothermal synthesis of ZnO nanowires[26] and repeated LPD of AuNPs (Figure 1A).[24] Arrays of ZnO nanowires were synthesized perpendicular to the silicon substrate to serve as skeletal frames. Initially the substrate was coated with a ZnO seed layer and then hydrothermal synthesis of ZnO nanowires was performed. The LPD process can be explained by the LaMer model and the DLVO theory.[27-31] Cl^- ions are displaced from $NaAuCl_4$ by hydrolysis and replaced by OH^- ions. Sodium citrate then initiates the reduction to Au anions.[32-34] During the reduction process, Au monomers are generated in the solution, and their concentration reaches the supersaturation point. When the Au monomer concentration exceeds the threshold for nucleation, the monomers go through burst nucleation and rapidly self-nucleate. This causes the concentration of monomers to drop immediately below the self-nucleation level. Then the diffusion of remaining monomers maintains the growth of Au NPs.[35] The size of particle is determined by the reaction pH level, chemical concentration, and reaction temperature.[36] In order to prevent rapid etching of ZnO nanowire, the pH of the precursor solution is initially adjusted to 9 by adding a NaOH solution. The diameter of fabricated AuNPs are held between 10 and 20 nm because citrate anions in the AuNP precursor solution cap the nanoparticles and prevent further aggregation of Au anions.[37] Ions in the solution surround the Au NPs and form the electric double layers (EDL). These layers generate repulsive force between Au NPs and obstruct their aggregation. If the gap between nanoparticles is instantaneously reduced by a thermodynamic force, the van der Waals force becomes larger than the EDL force, and the Au NPs will start to agglomerate.[36] Because the

initial pH level of the Au precursor solution is adjusted to 9, ZnO nanowire can endure through the nucleation process. During the Au NP growth, the precursor solution becomes more and more acidic, and ZnO nanowires dissolve away, but the nanowire shapes are preserved by the Au NPs that attached and formed clusters on the surface of the ZnO nanowires.

For comparison, AuNP-coated silicon substrates were fabricated in the absence of ZnO nanowires (2DNP-X where X is the number of LPD repetitions, Figure 1B). Because the thin ZnO-seed layer could not survive the AuNP synthesis process, we coated the Si wafer with 3-aminopropyltriethoxysilane (APTES) as an adhesion-promoting layer for AuNPs. The coating was done using a simple wet-chemical process. APTES functionalize the Si surface with amine groups, which allow the formation of chemical bonds with the citrates groups in the AuNP precursor solution.[38]

2DNP Substrate Characterization

Figure 2A shows SEM images of the top view of the 2DNP substrates. Sparely populated AuNPs with 10-20 nm diameters were observed on the wafer after the first LPD process (2DNP-1). As the number of the LPD repetitions increased, the number of nanoparticles observed on the wafer increased and the nanoparticles tended to aggregate forming sparsely dispersed clusters. Figures 2B-D show high-resolution SEM images of the cross-section and top views of the 2DNP-8 sample. Despite the increased synthesis time, the diameter of individual nanoparticles remained between 10 and 20 nm. The nanoparticle film height ranged between ca. 0.2 and 1 μm (Figure 2B) and the surface AuNP coverage is poor. Energy-dispersive spectroscopy (EDS) data of the device in Figure S1A and S1B agree with the SEM image data and shows the percentage of Au atoms increases with increasing LPD repetitions. The percentage of Au atoms is inversely

proportional to the percentage of Si atoms because the AuNPs on the surface cover the Si substrate.

In order to evaluate the SERS performance of the devices, SERS spectra were measured after incubation in 1-mM BT solution. As shown in Figure 2E, clear Raman peaks were observed at 999 cm^{-1} (in-plain ring-breathing mode), 1022 cm^{-1} (in-plain C-H bending mode), 1072 cm^{-1} (C-S stretching mode) and 1574 cm^{-1} (C-C stretching mode).[39] The SERS intensity was shown to increase with the number of LPD cycles (Figure 2F). After 8 LPD iterations, there is no sign of saturation.

Although the 2DNP substrates showed strong SERS hot spots, eight or more repetitions of the AuNP LPD are required to reach the enhancement level. This fabrication method is therefore time-consuming and inefficient. Additionally, this enhancement level showed no sign of saturation, indicating it is possible to improve the SERS beyond eight repetitions. Above all, the SEM image in Figure 2A shows the spatial uniformity is too poor for quantitative measurements.

3DNP Substrate Characterization

Nanowires were used as a basic framework to build a more spatially uniform SERS-enhanced substrate. ZnO nanowires were synthesized using the hydrothermal method, a simple way to synthesize nano-sized vertical structures illustrated in Figure 1A and 3A. Figure 3B shows the ZnO nanowire cross-section SEM image; the diameter and height of the ZnO nanowires were ca. 50 nm and 1 μm, respectively. After the synthesis of ZnO nanowires, AuNPs were adsorbed on the nanowires using the same method used to fabricate the 2DNP substrates. Due to the strong adsorption interaction between metal oxide and citrate anions, the AuNPs adhered to the surface of the ZnO nanowires without the addition of ATPES.[34] Figure 3A shows

a top view SEM image of the AuNP-coated ZnO nanowire. After 1 or 2 LPD repetitions (3DNP-1 and 3DNP-2), the shape of the ZnO nanowires were observed on the substrates and AuNPs coated the ZnO nanowire surface, shown in the cross section SEM image of 3DNP-1 in Figure 3C. Since the synthesis reaction occurred in liquid, the AuNPs formed on the top surfaces as well as the side-walls of the nanowires.

As the number of LPD repetitions increased, the ZnO nanowires dissolved and the sizes of the AuNP clusters increased. The etch rate of ZnO nanowires can be controlled by adjusting the acidity level of the AuNP precursor solution. In order to fabricate dense SERS substrates, we adjusted the initial pH of the precursor solution to 9, which is near the isoelectric point (i.e. no electric charges) of ZnO, and at this pH level, ZnO nanowires do not dissolve in the solution.[40] The pH level of the precursor solution was then dropped to ca. 5.5 during the synthesis process, causing the ZnO nanowires to gradually etch away through the synthesis iterations.

SEM images of 3DNP-1 through 3DNP-8 are shown in Figure 3A. The cross-section SEM images of 3DNP-0, 3DNP-1, and 3DNP-8 are shown in Figures 3B, 3C, and 3D, respectively. In Figure 3D, the presence of the vertical perforations created by dissolving ZnO nanowires are observed. This result is supported by the EDS data in Figure S2A and S2B, wherein the Zn:Au ratio decreased as the number of LPD repetitions increased. The observed Si atoms increased from one to four LPD repetitions due to the erosion of the ZnO nanowires causing exposure of the Si surface. For LPD repetitions greater than four, the ESD Si signal decreased because the AuNPs covered the Si substrate more densely. Figures 3E and 3F show high resolution SEM images of 3DNP-8. The diameters of individual NPs ranged between 10 and 20 nm, similar to the AuNPs on the flat 2DNP substrates. The clusters have many regions with sub-10-nm inter-particle gaps, which are properly sized to strongly enhance the electric field. The heights of

3DNP stacks were consistently thicker than the 2DNP films because the ZnO nanowires served as a skeletal frame for vertical deposition.

Figure 3G shows the SERS spectra of 3DNP substrates incubated in a 1-mM BT solution. Four clear peaks at 999, 1022, 1072 and 1574 cm^{-1} were detected, and the Raman intensities increased linearly up to three LPD repetitions as the nanoparticle density and the thickness of cluster also increased. After three LPD repetitions the Raman intensities were saturated. The SERS intensity of one repetition of AuNP deposition (3DNP-1) is larger than that of the flat 2DNP-6, which had six deposition repetitions of nanoparticles. Due to the efficient 3D vertical stacking of AuNPs, the 3DNP substrates benefit from larger surface areas and stronger particle-to-particle interactions. Additionally, the presence of vertical pathway holes allows the Raman intensities to achieve saturation after five iterations of nanoparticle deposition. The enhancement saturation is shown in Figure 3H and the enhancement factor was calculated to be 9.31×10^9. In comparison, our approach using dissolving ZnO nanowires showed a better EF (10^{10}) and spatial uniformity (7% RSD) than previously reported Si-nanowire-based platform (EF: 10^6-10^9; spatial uniformity: > 9 % RSD).[41-43]

Simulations of 3DNP substrates

In order to better understand the enhancing mechanism and the saturation effect, highly detailed numerical simulations were conducted. As shown in Figures 3D-F, the AuNPs were densely stacked along the ZnO vestiges, which acted as perforated optical pathways (Figure 4A). To replicate the 3D nanoparticle stacks with light paths in the simulator, rectangular stacks of reasonably well-aligned nanoparticles with inter-particle gap sizes varying between 8 and 22 nm were created. Considering the diameters of ZnO nanowires and AuNPs (Figure 4B), randomness was applied to their positions (deviation from the aligned positions with the standard deviation of

σ = 7 nm). Figure 4C shows the electric field intensity ($|E|^2$) distribution inside the blocks with various gap sizes. For small gap sizes (<11 nm) strong electric fields were present near the top regions of the structures. As the gap size increased, stronger electric fields appear deeper inside the blocks. This result verifies the ZnO vestiges play an important role as light-passing perforations. As shown in Figure 4D, the enhancement level reaches the peak values, saturates, and stays relatively constant when the particle-to-particle gap size ranges between 11 to 19 nm. The enhancement increased as the gap increases up to 10 nm and decreased above 20 nm. For gaps far below 10 nm, nanoparticles are more densely packed, and the excitation light reflects off the surface of the cluster and cannot interact with nanoparticles underneath the surface, and the overall enhancement is very weak. For gap sizes above 20 nm, the excitation light passes through the surface nanoparticles to deeper layers, however particle-to-particle interactions become too weak due to the larger gaps and overall enhancement is again very weak. Effective usage of excitation light and collection of Raman emission would lead to strong enhancement. For the gap sizes between 11 and 19 nm, there exists an optimal balance between the particle-to-particle interaction and a sufficiently large optical path, allowing the substrate to exhibit strong Raman enhancement. When gap sizes are smaller, for example, between 11 and 14 nm, we observe stronger particle-to-particle enhancement due to smaller gap sizes, but the penetration depth of excitation light is also shallow due to smaller gaps, and most of light-nanoparticle-molecule interactions occur near the top surface of the cluster. On the other hand, for larger gap sizes, especially between 16 and 19 nm, the particle-to-particle enhancement is weaker, but light-molecule interactions occurring in the deeper regions of the cluster also contribute to overall Raman emission due to the increased inter-particle gap sizes and make up the loss from the

weaker particle-to-particle interactions. As a result, the enhancement stays almost constant over the range of 11-19 nm, providing highly geometry-independent SERS performance.

In order to study the effect of the AuNP synthesis and LPD iterations in more detail, simulations at 12 AuNP thicknesses were conducted at 8, 15, and 22 nm particle-to-particle gap sizes. The substrate with small thickness does not sufficiently utilize the excitation light, wherein the electric field is strongest in the first layer of AuNPs and becomes smaller as the excitation light traveled toward the bottom layer (Figure S3A). As the thickness of the AuNP cluster is increased, a larger percentage of the laser excitation power is utilized and the total electromagnetic enhancement increased. The overall electromagnetic enhancement became saturated after the thickness exceeded a certain value, and the saturation thickness was highly correlated to the light penetration depth set by particle-to-particle gap size (Figure S3B). The observed trend matched well with the experimental results in Figure 3H.

In order to evaluate the sensitivity of the 3DNP substrates, samples were incubated in BT solution of various concentrations. As shown in Figure 5A, four clear SERS peaks were observed from the 1-μM, 1-nM, 1-pM, and 1-mM BT solutions. Intensities of the four Raman peaks decreased as the concentration of BT solution decreased (Figure 5B). The 3DNP substrates effectively absorb the excitation light and generate stronger Raman enhancement, which allows the detection of picomolar concentrated BT.

The 3DNP substrate exhibits excellent spatial uniformity. As shown in Figures 5C and S4A, the substrate surface looks uniformly black. The use of a newly designed mechanical stirrer, which improved temperature and chemical concentration uniformity in the precursor solution, combined with repetitions of the Au synthesis resulted in a uniform AuNP layer over the entire substrate thick enough to saturate SERS emissions. As studied in numerical simulation

section, the thick AuNP layers made saturated electromagnetic enhancement and overstacked layers didn't affect to saturated SERS emissions. The SERS intensity almost reached the saturated value after third Au synthesis repetition (Figure 3H), we conducted five more Au synthesis process in order to get saturated signal in entire substrate. The spatial uniformity of the SERS intensity across the 4-inch wafer was excellent and had a the relative standard deviation (RSD) below 13% (Figures 5D, 5E and S4B-S4E). Moreover, the uniformity of the SERS intensity within an area of 4 × 4 mm^2, a typical size widely used for commercial SERS substrates, showed a RSD less than 7% (Figure S4F and S4G), which is approximately six times better than the flat 2DNP substrates (RSD > 40%) (Figure S4H and S4I). Moreover, the device is larger and more uniform than previous works using complex fabrication processes (Figure S5 and Table S1).[21, 44-58] The wafer-scale uniformity and strong enhancement were achieved using precursor-based fabrication processes that can be easily applied to large scale productions without significant setup investment. These desirable properties can provide high usability for practical applications such as quantitative monitoring of biological molecules.

We also measured SERS intensities of BT as a function of incidence angle between 0° and 80° (Figures 5F and 5G). The intensity maxed out at 0° and remained almost constant up to 30°, at which the intensity reduced by 6.5%. The perceived view of the 3D-stacked particle-gap geometry stays uniform to a good extent even up to a viewing angle of 30°, and this reduces angle dependence. If the incidence angle becomes larger than 30°, the excitation laser is not tightly focused anymore, and the cluster geometry viewed at an angle over 30° becomes similar to an excessively packed AuNP cluster with no gaps. The SERS intensity would decrease. The dominant Raman peaks, although they became much weaker, were still detectable at 80°. This

high angle independence can also be useful for practical applications that require quantitative measurements.

Quantitative application of 3DNP substrates

As a demonstration of quantitative measurements, the concentrations of adenine in solution were determined experimentally. The SERS intensity of 3DNP-8 substrates in adenine at four concentrations (10 nM, 100 nM, 1 μM, and 10 μM) were measured. As shown in Figure 5D, the substrate showed excellent uniformity throughout the entire wafer, and this is a very important property for substrates used in quantitative measurements. The clear Raman peak observed at 735 cm^{-1}, whose intensity was linearly proportional to the concentration of adenine solutions (Figure 6A and 6B), was measured. The relationship between the concentration and the intensity represented by the line shown in Figure 6B follows $I = 2.45\times10^{6}\cdot C^{0.4302} - 73.38$, where I and C are the SERS intensity and molar concentration in solution, respectively. Next, we incubated five 3DNP-8 substrates in 60-nM, 200-nM and 4-μM adenine solutions and calculated the concentrations to 63.1 nM, 213.3 nM and 3.71 μM, respectively. These results, shown in Figure 6C, match the given concentrations accurately within 10%.

CONCLUSIONS

3D-stacked AuNP clusters with light-passing perforations were fabricated, and their use as a high-performance SERS substrate for quantitative sensing was demonstrated. Simple hydrothermal synthesis produced ZnO nanowires, which served as a template for efficient fabrication of a 3D substrate, and AuNPs were deposited by repeating LPD cycles. Due to the nanowire-generated light-passing perforations and 3D stacks made of properly sized nanoparticles and inter-particle gaps, the Raman-enhancing performance of the substrate is

highly independent of the final geometry of the nanoparticle clusters and shows high enhancement and uniformity across the wafer, which is confirmed by both experimental measurements and numerical simulations. The enhancement factor was calculated to be approximately 9.31×10^9 and the 3DNP substrate clearly detected SERS peaks in 1-pM BT solution. Also, the 3DNP substrate measured the concentration of a 60-nM adenine solution within 10%. This relatively simple approach can be widely adapted by most wet labs and is also suitable for large-scale productions, suggesting a promising way to implement commercial SERS substrates for biological and chemical sensing applications.

MATERIALS AND METHODS

Chemicals. Chemicals used for this investigation include the following: zinc acetate dihydrate ($Zn(CH_3COO)_2 \cdot 2H_2O$, Sigma Aldrich, ≥98%), ethanol, (CH_3CH_2OH, Sigma Aldrich, 200 proof), zinc nitrate hexahydrate ($Zn(NO_3)_2 \cdot 6H_2O$, Sigma Aldrich, 98%), polyethyleneimine (PEI, $(C_2H_5N)_n$, Sigma Aldrich, average M_w ~800), hexamethylenetetramine (HMTA, $C_6H_{12}N_4$, Sigma Aldrich, ≥ 99%), sodium tetrachloroaurate(III) dihydrate, ($NaAuCl_4 \cdot 2H_2O$, Sigma Aldrich, ≥99%), sodium citrate dihydrate ($HOC(COONa)(CH_2COONa)_2 \cdot 2H_2O$, Sigma Aldrich, ≥ 99%), sodium hydroxide (NaOH, Sigma Aldrich, ≥ 98%), 3-aminopropyltriethoxysilane, (APTES, $H_2N(CH_2) \cdot 3Si(OC_2H_5)_3$, Sigma Aldrich, ≥ 99%) and benzenethiol (BT, C_6H_5SH, Sigma Aldrich, ≥98%).

Fabrication of 2DNP substrates. A bare Si wafer was immersed in APTES for 15 minutes to ensure the adhesion of the synthesized AuNPs to the substrate. The substrate was then placed in the AuNP precursor solution in a convection oven at 90˚C for 1 hour. The precursor

solution was prepared from 1 mM sodium tetrachloroaurate (III) dihydrate and 200 μM sodium citrate dihydrate in DI water. 0.1 M NaOH aqueous solution was added until the resulting pH of the solution was 9.[33] The LPD process was repeated between 1 and 8 times for AuNP films of increasing thichkness (2DNP-1, 2DNP-2, …, and 2DNP-8). The higher the number of repetition, the thicker the AuNP film. The substrates were washed with DI water and ethanol to remove excess salt and carbon compounds.

Fabrication of 3DNP substrates. A ZnO seed solution consisting of 5 mM zinc acetate dihydrate in ethanol was coated on a bare Si substrate and then annealed on a hot plate at 350˚C for 20 minutes to ensure seed adhesion to the silicon.[59] The substrate was then placed inside the ZnO precursor solution, which consisted of 25 mM zinc nitrate hexahydrate, 25 mM HMTA and 5 mM PEI in DI water for 2.5 hours at 95˚C in a convection oven.[26] The substrate was then taken out of the solution, rinsed with DI water, and annealed on a hot plate at 350˚C for 20 minutes. In order to synthesize AuNP on ZnO nanowires, the silicon substrates with ZnO nanowires were placed into a AuNP precursor solution. The solution was heated to 90˚C for 1 hour and the process was repeated between 1 and 8 times to create a dense AuNP film (3DNP-1, 3DNP-2, … and 3DNP-8). The substrates were then washed with DI water and ethanol to remove excess salt and carbon compounds.

SERS measurements of benzenethiol (BT). All substrates were incubated in a 1 mM BT ethanol solution for 5 hours. Additionally, ZnO nanowire substrates coated with 5 repetitions of gold nanoparticles were incubated in 1 μM, 1 nM and 1 pM BT solution for 5 hours. The samples were taken out of the BT solution, rinsed with ethanol and dried using nitrogen gas. Measurements were taken using a Raman microscope (inVia, Renishaw, United Kingdom) with 20× magnitude objective lens with 1.25-μm spot size and 0.07 mW of 785-nm laser for 100 s.

SERS measurements for evaluation of spatial uniformity and angle independence. To evaluate substrate uniformity, a 4-inch wafer and a 4 mm × 4 mm piece of 3DNP-8 (Si wafer with ZnO nanowire substrate coated with 8 repetitions of AuNP LPD), in addition to a 4 mm × 4 mm piece of 2DNP-8 (Si substrate coated with 8 repetitions of AuNP LPD) were incubated in 1 mM BT solution. The samples were scanned at a step size of 0.5 μm and 0.1 μm, respectively, using 5× magnitude objective lens with 4.15-μm spot size and 0.77 mW of 785-nm laser for 3 s. To test angle independence, 1 mM BT incubated 3DNP-8 was prepared. The SERS intensity of the substrate was measured at various incidence angles from flat to 80° using 0.07 mW of 785-nm laser for 100 s.

Numerical analysis. Simulations were performed using a commercial program (Lumerical FDTD Solutions 2016a, Lumerical Solutions Inc., United Kingdom) based on a 3D Finite difference time domain (FDTD) algorithm.[60] The 14 nm diameter AuNPs of 8 by 8 rectangular arrays, assumed to be placed with 7 nm uniform random distribution from the lattice point, were stacked on the top of Si substrate (refractive index, n = 3.5).[61] In this calculation, periodic boundaries and perfectly matched layers were used and the minimum computational cell size was 1 nm^3. The linearly polarized 800 nm wavelength source was illuminated from the top.

SERS measurements of adenine. The SERS substrate was diced into 2×2-mm^2 chips for testing, and the SERS spectra were measured using 20× magnitude objective lens with 1.25-μm spot size and 0.07 mW of 785-nm laser for 100 s. We used a new chip for every measurement. For calibration measurements, we incubated four chips in 10-nM, 100-nM, 1-μM, and 10-μM adenine solution for 5 hours and measured corresponding Raman spectra. To obtain the measurement accuracy of the SERS devices, we incubated another set of 2×2-mm^2 chips in three

different adenine concentration levels of 60-nM, 200-nM and 4-μM and measured their SERS spectra under the same measurement condition.

FIGURES

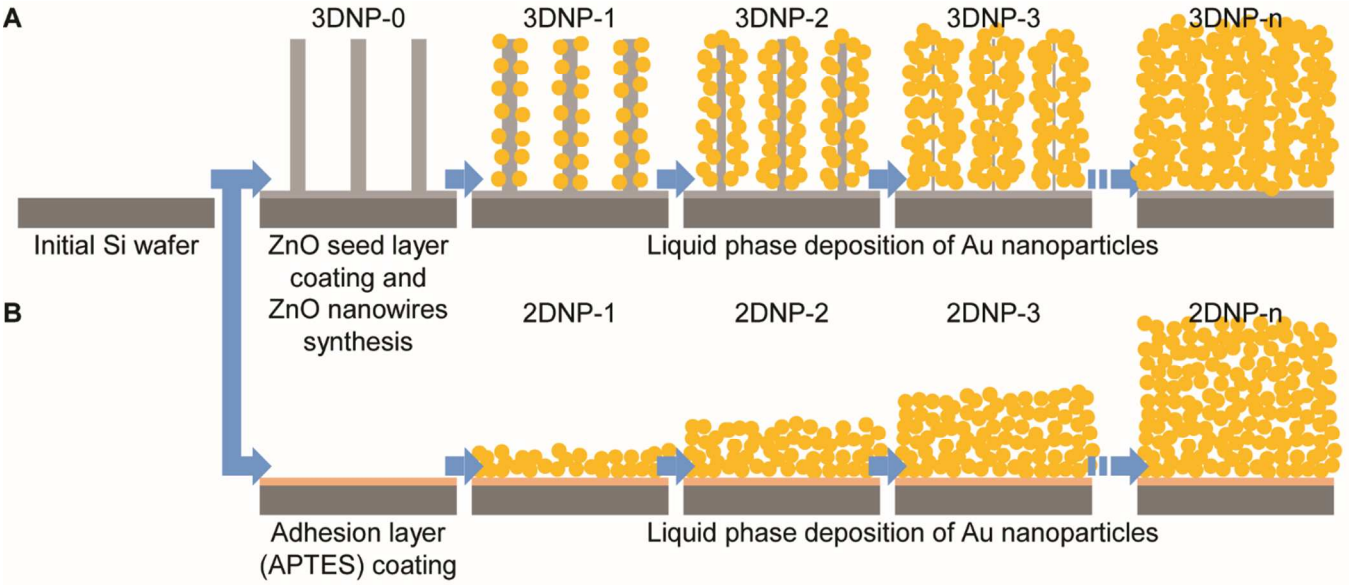

Figure 1. A schematic of the fabrication process for (A) 3D-stacked gold-nanoparticle clusters built on a Si wafer using ZnO nanowires (3DNP samples) and (B) gold-nanoparticle coated Si wafer (2DNP samples).

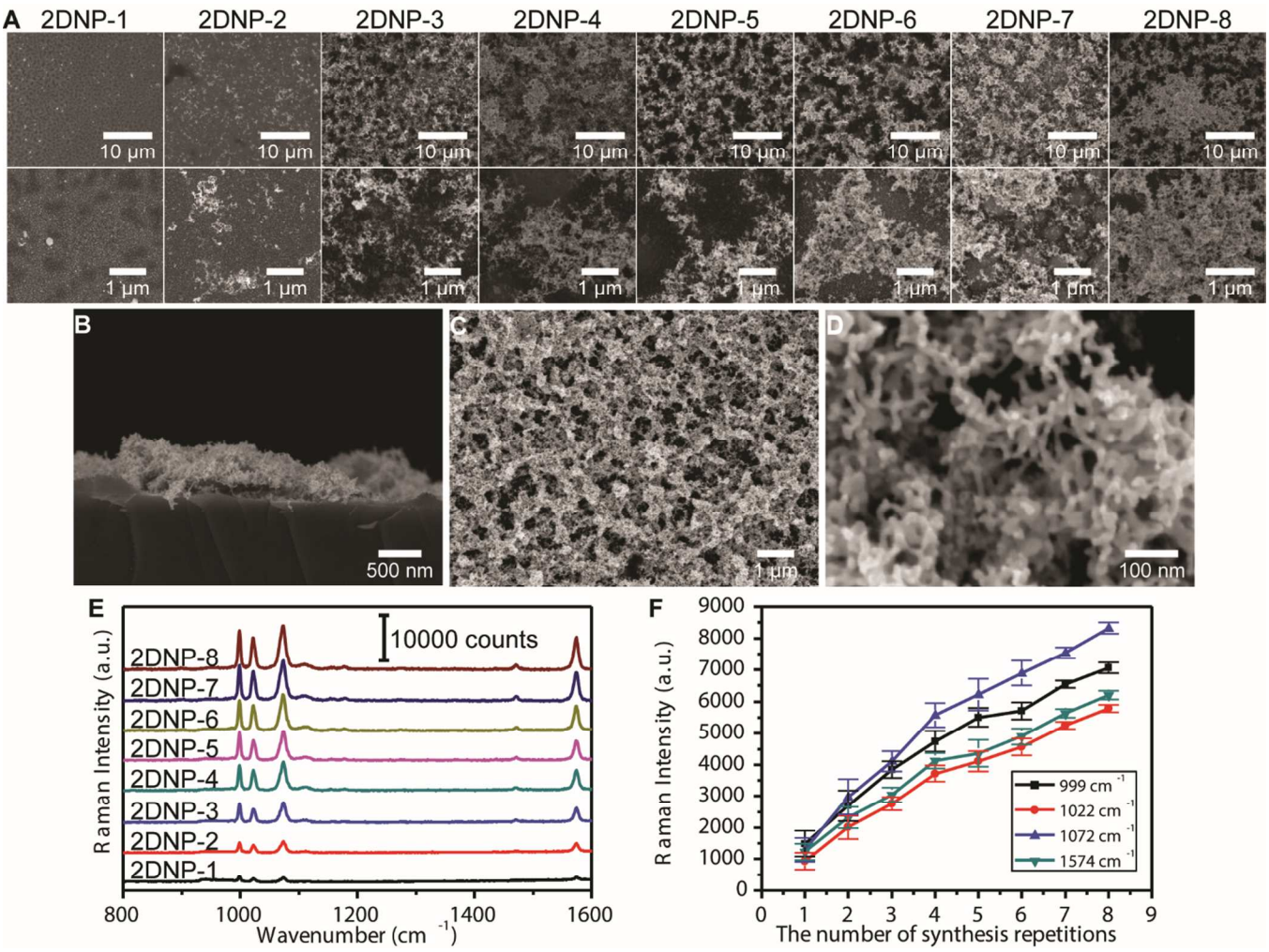

Figure 2. SEM images of (A) the top view of the gold nanoparticle film coated substrates (2DNP substrates) with varying AuNP LPD repetitions (1-8); (B) the cross sectional view and (C, D) top views of 2DNP-8; (E) SERS spectra of 2DNP-1 through 2DNP-8 1 mM benzenethiol solutions and (F) the Raman intensities at wavenumbers of 999, 1022, 1072 and 1574 cm^{-1} measured on the 2DNP substrates as a function of synthesis repetitions.

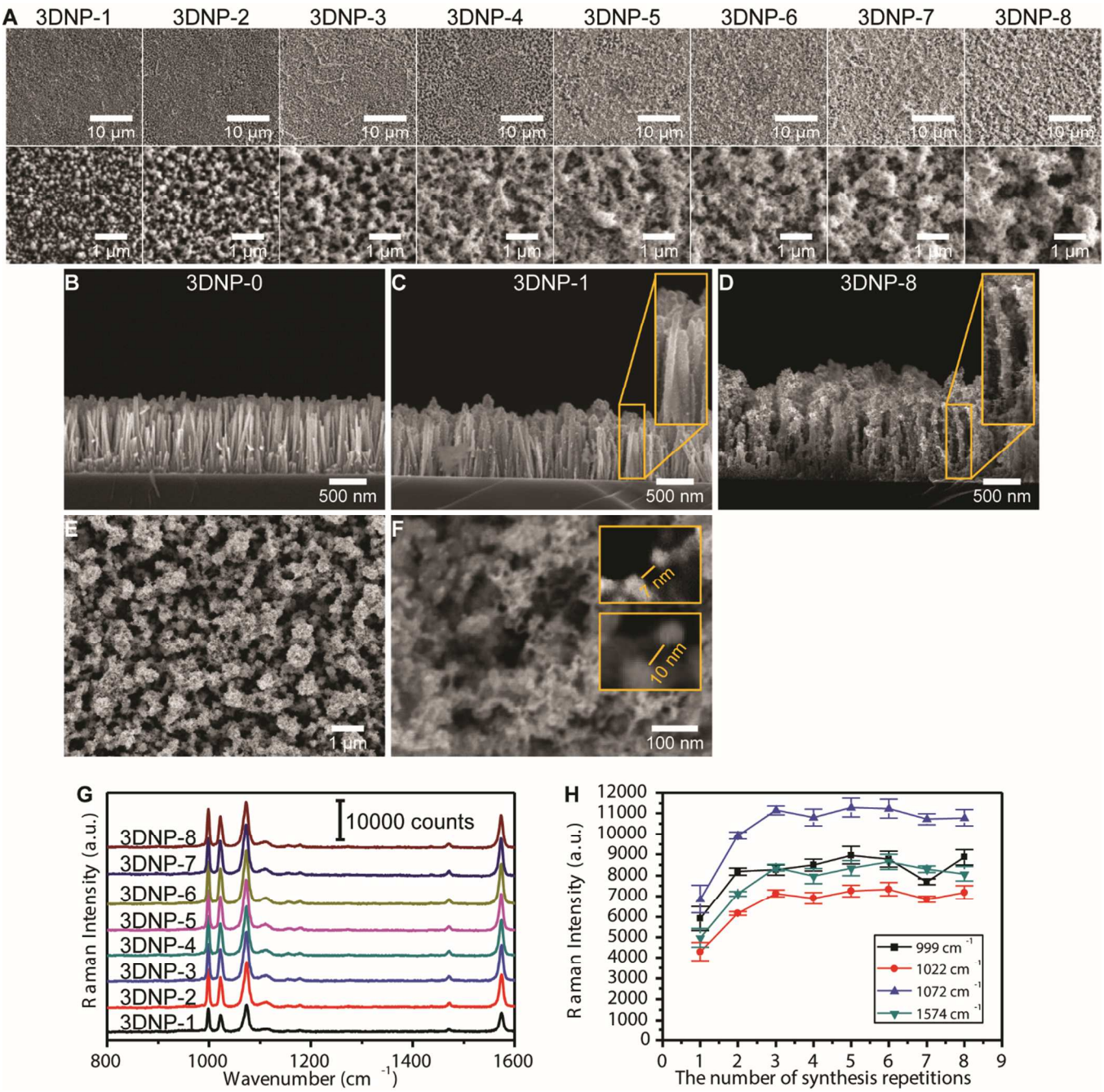

Figure 3. Top view SEM images of 3DNP substrates, which were made of ZnO nanowires grown on a Si wafer substrate and repetitive AuNP LPD processes (3DNP substrates); (B-D) cross sectional views of the ZnO nanowires before gold nanoparticle deposition (3DNP-0) and after Au NPs deposition (3DNP-1 and 3DNP-8); (E,F) top views of the of the 3DNP-8 sample;

(G) SERS spectra of 1 mM benzenethiol solution and (H) Raman intensities at 999, 1022, 1072 and 1574 cm^{-1} measured on 3DNP substrates with variation in LPD repetitions.

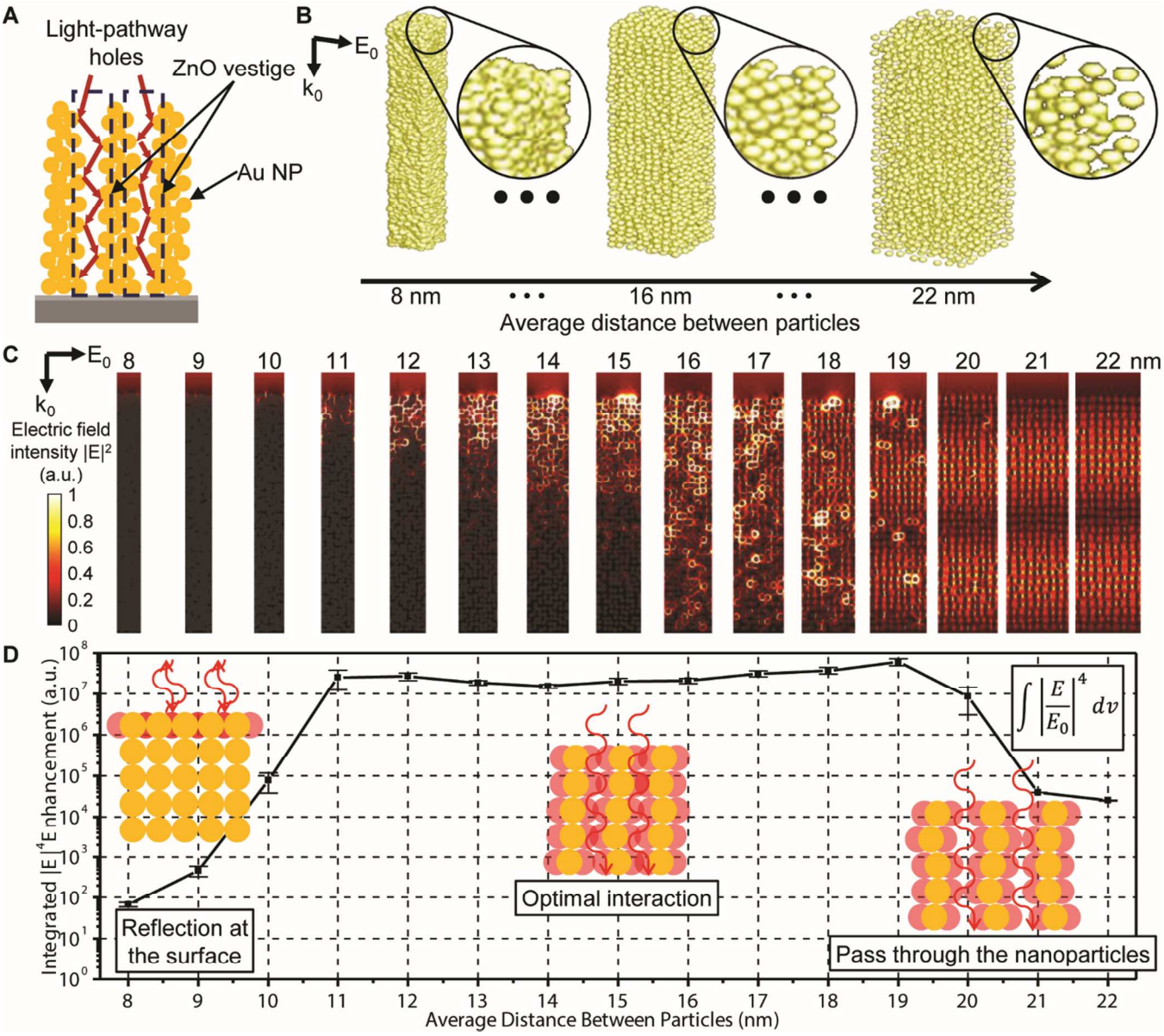

Figure 4. (A) A schematic illustration of the nanoparticle clusters with light-passing perforations of the 3DNP substrates; (B) geometry of 3DNP substrate for numerical simulation; (C) numerical simulation results of electric field intensity ($|E|^2$) distribution with various gap sizes

and (D) the relationship between integrated $|E|^4$ enhancement and the particle-to-particle gap size.

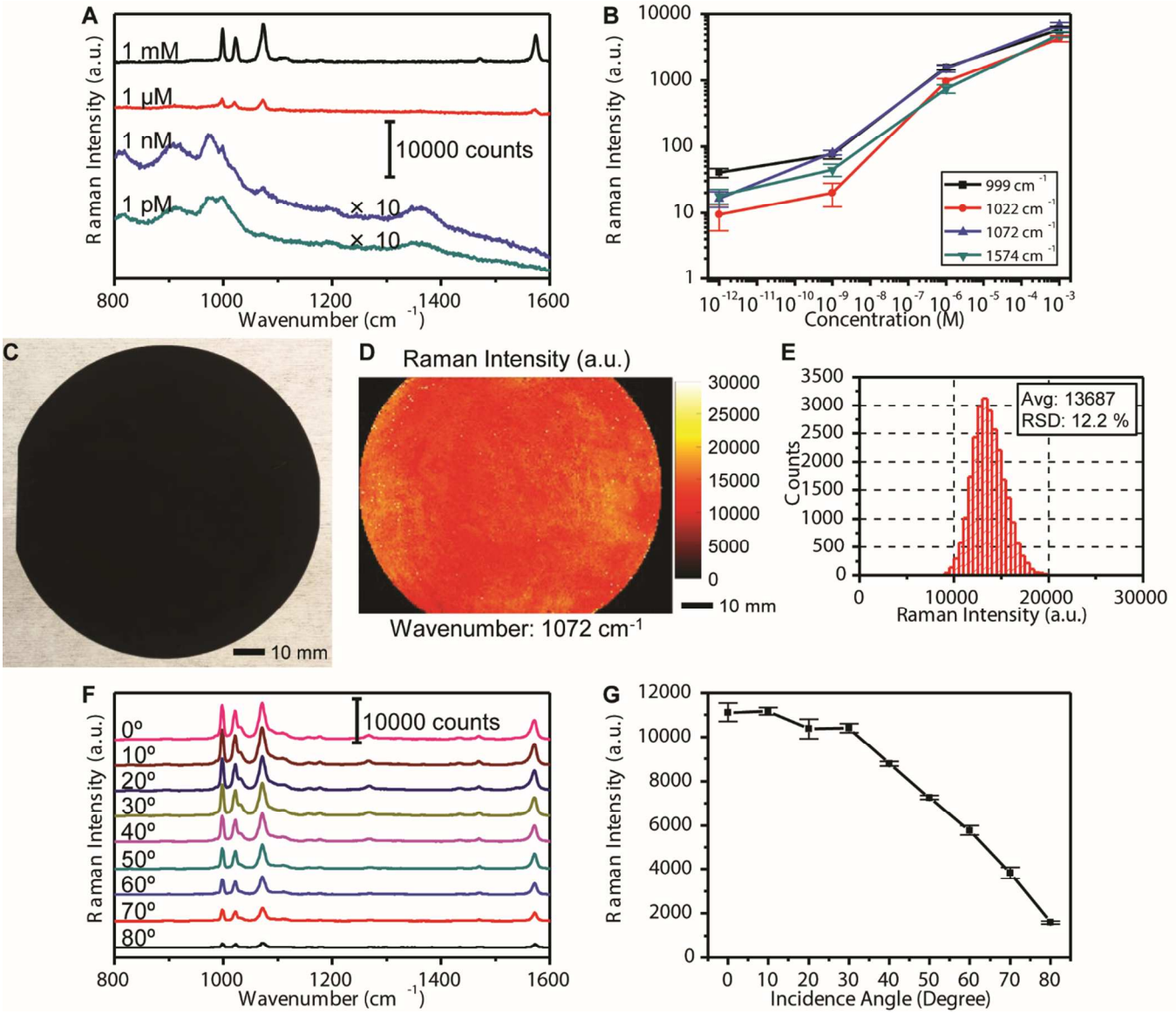

Figure 5. (A) SERS spectra of 1 mM, 1 μM, 1 nM and 1 pM benzenethiol solution and (B) the SERS intensity at 999, 1022, 1072 and 1574 cm^{-1} with various concentrations of benzenethiol solution; (C) photo of 3D stacked AuNPs synthesized on 4 inch Si wafer; (D) 2D mapping and (E) intensity distribution of 1072 cm^{-1} peak of 1 mM benzenethiol incubated 3D stacked AuNP

synthesized on 4 inch Si wafer; (F) SERS spectra of 1 mM benzenethiol incubated 3D stacked AuNP substrate with various incidence angles and (G) the relationship between SERS intensity and incidence angle.

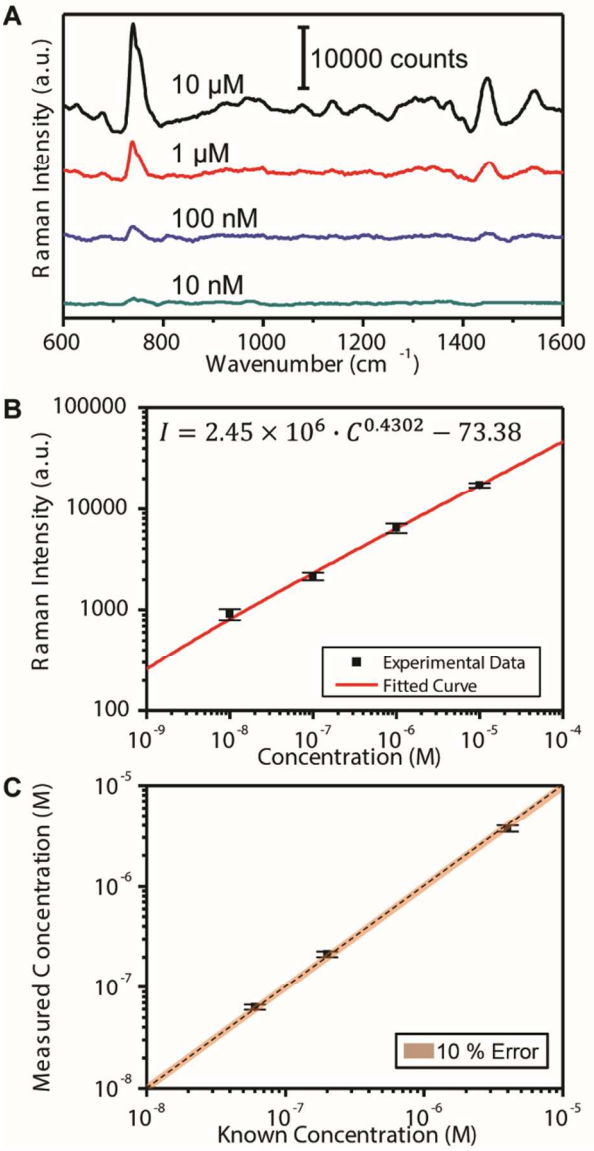

Figure 6. (A) Reference SERS spectra of 10 μM, 1 μM, 100 nM and 10 nM adenine solutions measured using 3DNP-8; (B) the experimentally measured reference relationship between the concentration of adenine solution and SERS intensity; (C) concentration readouts for adenine solutions using 3DNP-8.

ASSOCIATED CONTENT

Supporting Information.

(1) EDS data of 2DNP substrates as a function of synthesis repetition. (2) EDS data of 3DNP substrates as a function of synthesis repetition. (3) Numerically simulated electric field intensity ($|E|^2$) distribution inside 3D stacks for various gap sizes and as a function of the layer depth. (4) 2D Raman mapping and statistical distributions of Raman enhancement measured on a 2DNP-8 substrate and 4-inch wafer-sized 3DNP substrate. (5) SERS performance comparison with previous large and uniform SERS substrates. (6) Enhancement factor calculation for 3DNP substrates. This material is available free of charge via the Internet at http://pubs.acs.org.

Corresponding Author

*E-mail: hchoo@caltech.edu

Author Contributions

The manuscript was written through contributions of all authors. All authors have given approval to the final version of the manuscript.

Notes

The authors declare no competing financial interest.

ACKNOWLEDGMENT

The research was funded by Samsung Grand Research Opportunity and Heritage Medical Research Institute Inaugural Principle Investigator Program. The authors also thank Professor Inkyu Park for helpful discussion on the AuNP synthesis.

ABBREVIATIONS

SERS: surface-enhanced Raman spectroscopy; LPD: liquid phase deposition; FDTD: finite-difference time-domain; NP: nanoparticle; AuNP: gold nanoparticles; 2DNP: flat gold-nanoparticle-layer substrate; 3DNP: 3D-stacked gold-nanoparticle substrate fabricated using ZnO nanowires; APTES: 3-aminopropyltriethoxysilane; SEM: scanning electron microscope; EDS: energy-dispersive spectroscopy; BT: benzenethiol; RSD: relative standard deviation; PEI: polyethyleneimine; HMTA: hexamethylenetetramine.

REFERENCES

1. Nie, S. M.; Emery, S. R. Probing Single Molecules and Single Nanoparticles by Surface-Enhanced Raman Scattering. *Science* **1997,** *275*, 1102-1106.

2. Fleischmann, M.; Hendra, P. J.; McQuilla. A.J. Raman Spectra of Pyridine Adsorbed at a Silver Electrode. *Chem. Phys. Lett.* **1974,** *26*, 163-166.

3. White, P. L.; Hibbitts, S. J.; Perry, M. D.; Green, J.; Stirling, E.; Woodford, L.; McNay, G.; Stevenson, R.; Barnes, R. A. Evaluation of a Commercially Developed Semiautomated PCR-Surface-Enhanced Raman Scattering Assay for Diagnosis of Invasive Fungal Disease. *J. Clin. Microbiol.* **2014,** *52*, 3536-3543.

4. Campion, A.; Kambhampati, P. Surface-Enhanced Raman Scattering. *Chem. Soc. Rev.* **1998,** *27*, 241-250.

5. Schlucker, S. Surface-Enhanced Raman Spectroscopy: Concepts and Chemical Applications. *Angew. Chem. Int. Ed.* **2014,** *53*, 4756-4795.

6. Kambhampati, P.; Child, C. M.; Foster, M. C.; Campion, A. On the Chemical Mechanism of Surface Enhanced Raman Scattering: Experiment and Theory. *J. Chem. Phys.* **1998,** *108*, 5013-5026.

7. Alonso-Gonzalez, P.; Albella, P.; Schnell, M.; Chen, J.; Huth, F.; Garcia-Etxarri, A.; Casanova, F.; Golmar, F.; Arzubiaga, L.; Hueso, L. E.; Aizpurua, J.; Hillenbrand, R. Resolving the Electromagnetic Mechanism of Surface-Enhanced Light Scattering at Single Hot Spots. *Nat. Comm.* **2012,** *3*, 7.

8. Tong, L. M.; Zhu, T.; Liu, Z. F. Approaching the Electromagnetic Mechanism of Surface-Enhanced Raman Scattering: from Self-Assembled Arrays to Individual Gold Nanoparticles. *Chem. Soc. Rev.* **2011,** *40*, 1296-1304.

9. Sun, M. T.; Wan, B. S.; Liu, Y. J.; Jia, Y.; Xu, H. X. Chemical Mechanism of Surface-Enhanced Resonance Raman Scattering via Charge Transfer in Pyridine-Ag-2 Complex. *J. Raman Spectrosc.* **2008,** *39*, 402-408.

10. Zayak, A. T.; Hu, Y. S.; Choo, H.; Bokor, J.; Cabrini, S.; Schuck, P. J.; Neaton, J. B. Chemical Raman Enhancement of Organic Adsorbates on Metal Surfaces. *Phys. Rev. Lett.* **2011,** *106*, 083003.

11. Zayak, A. T.; Choo, H.; Hu, Y. S.; Gargas, D. J.; Cabrini, S.; Bokor, J.; Schuck, P. J.; Neaton, J. B. Harnessing Chemical Raman Enhancement for Understanding Organic Adsorbate Binding on Metal Surfaces. *J. Phys. Chem. Lett.* **2012,** *3*, 1357-1362.

12. Fang, J. X.; Yi, Y.; Ding, B. J.; Song, X. P. A Route to Increase the Enhancement Factor of Surface Enhanced Raman Scattering (SERS) via a High Density Ag Flower-Like Pattern. *Applied Phys. Lett.* **2008,** *92*, 131115.

13. Braun, G.; Lee, S. J.; Dante, M.; Nguyen, T. Q.; Moskovits, M.; Reich, N. Surface-Enhanced Raman Spectroscopy for DNA Detection by Nanoparticle Assembly onto Smooth Metal Films. *J. Am. Chem. Soc.* **2007,** *129*, 6378-6379.

14. Tang, H. B.; Meng, G. W.; Huang, Q.; Zhang, Z.; Huang, Z. L.; Zhu, C. H. Arrays of Cone-Shaped ZnO Nanorods Decorated with Ag Nanoparticles as 3D Surface-Enhanced Raman Scattering Substrates for Rapid Detection of Trace Polychlorinated Biphenyls. *Adv. Funct. Mater.* **2012,** *22*, 218-224.

15. Liu, Y.; Zhang, X. H.; Su, J.; Li, H. X.; Zhang, Q.; Gao, Y. H. Ag Nanoparticles@ZnO Nanowire Composite Arrays: an Absorption Enhanced UV Photodetector. *Opt. Express,* **2014,** *22*, 30148-30155.

16. Dai, Z. G.; Wang, G. M.; Xiao, X. H.; Wu, W.; Li, W. Q.; Ying, J. J.; Zheng, J. F.; Mei, F.; Fu, L.; Wang, J.; Jiang, C. Z. Obviously Angular, Cuboid-Shaped TiO_2 Nanowire Arrays Decorated with Ag Nanoparticle as Ultrasensitive 3D Surface-Enhanced Raman Scattering Substrates. *J. Phys. Chem. C* **2014,** *118*, 22711-22718.

17. Bai, F.; Li, M. C.; Fu, P. F.; Li, R. K.; Gu, T. S.; Huang, R.; Chen, Z.; Jiang, B.; Li, Y. F. Silicon Nanowire Arrays Coated with Electroless Ag for Increased Surface-Enhanced Raman Scattering. *APL Mater.* **2015,** *3*, 056101.

18. Fu, S. Y.; Hsu, Y. K.; Chen, M. H.; Chuang, C. J.; Chen, Y. C.; Lin, Y. G. Silver-Decorated Hierarchical Cuprous Oxide Micro/Nanospheres as Highly Effective Surface-Enhanced Raman Scattering Substrates. *Opt. Express* **2014,** *22*, 14617-14624.

19. Zhou, Q. T.; Meng, G. W.; Huang, Q.; Zhu, C. H.; Tang, H. B.; Qian, Y. W.; Chen, B.; Chen, B. S. Ag-Nanoparticles-Decorated NiO-Nanoflakes Grafted Ni-Nanorod Arrays Stuck out of Porous AAO as Effective SERS Substrates. *Phys. Chem. Chem. Phys.* **2014,** *16*, 3686-3692.

20. Zhu, W. Q.; Banaee, M. G.; Wang, D. X.; Chu, Y. Z.; Crozier, K. B. Lithographically Fabricated Optical Antennas with Gaps Well Below 10 nm. *Small* **2011,** *7*, 1761-1766.

21. Zhang, P.; Yang, S.; Wang, L.; Zhao, J.; Zhu, Z.; Liu, B.; Zhong, J.; Sun, X. Large-Scale Uniform Au Nanodisk Arrays Fabricated via X-Ray Interference Lithography for Reproducible and Sensitive SERS Substrate. *Nanotechnology* **2014,** *25* 245301.

22. Tang, X.; Cai, W.; Yang, L.; Liu, J. Highly Uniform and Optical Visualization of SERS Substrate for Pesticide Analysis Based on Au Nanoparticles Grafted on Dendritic Alpha-Fe_2O_3. *Nanoscale* **2013,** *5*, 11193-11199.

23. Pazos-Perez, N.; Ni, W.; Schweikart, A.; Alvarez-Puebla, R. A.; Fery, A.; Liz-Marzan, L. M. Highly Uniform SERS Substrates Formed by Wrinkle-Confined Drying of Gold Colloids. *Chem. Sci.* **2010,** *1*, 174-178.

24. Acosta, B.; Smolentseva, E.; Beloshapkin, S.; Rangel, R.; Estrada, M.; Fuentes, S.; Simakov, A. Gold Supported on Ceria Nanoparticles and Nanotubes. *Appl. Catal. A-Gen.* **2012,** *449*, 96-104.

25. Wei, S.; Zheng, M.; Xiang, Q.; Hu, H.; Duan, H.; Optimization of the Particle Density to Maximize the SERS Enhancement Factor of Periodic Plasmonic Nanostructure Array. *Opt. Express* **2016,** 24, 20613-20620.

26. Law, M.; Greene, L. E.; Johnson, J. C.; Saykally, R.; Yang, P. D. Nanowire Dye-Sensitized Solar Cells. *Nat. Mat.* **2005,** *4*, 455-459.

27. La Mer, V.K.; Nucleation in Phase Transitions. *Ind. Eng. Chem.* **1952,** 44, 1270-1277.

28. La Mer, V.K.; Dinegar, R.H.; Theory, Production and Mechanism of Formation of Monodispersed Hydrosols, *J. Am. Chem. Soc.* **1950,** 72, 4847-4854.

29. Derjaguin, B.; A Theory of Interaction of Particles in Presence of Electric Double-Layers and the Stability of Lyophobe Colloids and Disperse Systems. *Acta Phys. Chim.* **1939,** 10, 333-346.

30. Derjaguin, B.; Landau, L.D.; Theory of the Stability of Strongly Charged Lyophobic Sols and of the Adhesion of Strongly Charged Particles in Solutions of Electrolytes. *Acta Phys. Chim.* **1941,** 14, 633-662.

31. Verwey, E.J.W.; Theory of the Stability of Lyophobic Colloids. *J. Phys. Chem.* **1947,** 51, 631-636.

32. Moreau, F.; Bond, G. C.; Taylor, A. O. Gold on Titania Catalysts for the Oxidation of Carbon Monoxide: Control of pH During Preparation with Various Gold Contents. *J. Cataly.* **2005,** *231*, 105-114.

33. Lim, M. A.; Lee, Y. W.; Han, S. W.; Park, I. Novel Fabrication Method of Diverse One-Dimensional Pt/ZnO Hybrid Nanostructures and Its Sensor Application. *Nanotechnology* **2011,** *22*, 035601.

34. Haruta, M. Nanoparticulate Gold Catalysts for Low-Temperature CO Oxidation. *J. New Mater. Electrochem. Syst.* **2004,** *7*, 163-172.

35. Polte, J.; Fundamental Growth Principles of Colloidal Metal Nanoparticles - A New Perspective. *CrystEngComm.* **2015,** 17, 6809-6830.

36. Piella, J.; Bastus, N.G.; Puntes,V.; Size-Controlled Synthesis of Sub-10-nanometer Citrate-Stabilized Gold Nanoparticles and Related Optical Properties. *Chem. Mater.* **2016,** 28, 1066-1075.

37. Zhao, L. L.; Jiang, D.; Cai, Y.; Ji, X. H.; Xie, R. U.; Yang, W. S. Tuning the Size of Gold Nanoparticles in the Citrate Reduction by Chloride Ions. *Nanoscale* **2012,** *4*, 5071-5076.

38. Castillo, F.; Perez, E.; de la Rosa, E., Adsorption of Gold Nanoparticles on Silicon Substrate and Their Application in Surface Enhancement Raman Scattering. *Rev. Mex. Fis.* **2011,** *57*, 61-65.

39. Joo, T. H.; Kim, M. S.; Kim, K. Surface-Enhanced Raman-Scattering of Benzenethiol in Silver Sol. *J. Raman Spectrosc.* **1987,** *18*, 57-60.

40. Zang, J.; Li, C. M.; Cui, X.; Wang, J.; Sun, X.; Dong, H.; Sun, C. Q. Tailoring Zinc Oxide Nanowires for High Performance Amperometric Glucose Sensor. *Electroanalysis* **2007,** *19*, 1008-1014.

41. Huang, J.-A.; Zhao, Y.-Q.; Zhang, X.-J.; He, L.-F.; Wong, T.-L.; Chui, Y.-S.; Zhang, W.-J.; Lee, S.-T.; Ordered Ag/Si Nanowires Array: Wide-Range Surface-Enhanced Raman Spectroscopy for Reproducible Biomolecule Detection. Nano Lett. 2013, 13, 5039-5045.

42. Akin, M.S.; Yilmaz, M.; Babur, E.; Ozdemir, B.; Erdogan, H.; Tamer, U.; Demirel, G.; Large Area Uniform Deposition of Silver Nanoparticles Through Bio-Inspired Polydopamine Coating on Silicon Nanowire Arrays for Practical SERS Applications. J. Mater. Chem. B 2014, 2, 4894-4900.

43. Yang, X.; Zhong, H.; Zhu, Y.; Shen, J.; Li. C.; Ultrasensitive and Recyclable SERS Substrate Based on Au-Decorated Si Nanowire Arrays. Dalton Trans., 2013, 42, 14324-14330.

44. Zhang, L.; Guan, C. R.; Wang, Y.; Liao, J. H. Highly Effective and Uniform SERS Substrates Fabricated by Etching Multi-Layered gold Nanoparticle Arrays. *Nanoscale* **2016,** *8*, 5928-5937.

45. Kanipe, K. N.; Chidester, P. P. F.; Stucky, G. D.; Moskovits, M. Large Format Surface-Enhanced Raman Spectroscopy Substrate Optimized for Enhancement and Uniformity. *ACS Nano* **2016,** *10*, 7566-7571.

46. Xu, Z. D.; Jiang, J.; Wang, X. H.; Han, K.; Ameen, A.; Khan, I.; Chang, T. W.; Liu, G. L., Large-area, Uniform and Low-Cost Dual-Mode Plasmonic Naked-Eye Colorimetry and SERS Sensor with Handheld Raman Spectrometer. *Nanoscale* **2016,** *8*, 6162-6172.

47. Zhu, C. H.; Meng, G. W.; Zheng, P.; Huang, Q.; Li, Z. B.; Hu, X. Y.; Wang, X. J.; Huang, Z. L.; Li, F. D.; Wu, N. Q. A Hierarchically Ordered Array of Silver-Nanorod Bundles

for Surface-Enhanced Raman Scattering Detection of Phenolic Pollutants. *Adv. Mater.* **2016,** *28*, 4871-4876.

48. Zhou, J. H.; Zhu, F.; Wang, Y.; Wang, T. One-Step Green Synthesis of High Uniform SERS Substrate Based on Au Nanoparticles Grown on Ge Wafer. *Chem. Phys. Lett.* **2015,** *627*, 96-100.

49. Wang, Y. W.; Kao, K. C.; Wang, J. K.; Mou, C. Y. Large-Scale Uniform Two-Dimensional Hexagonal Arrays of Gold Nanoparticles Templated from Mesoporous Silica Film for Surface-Enhanced Raman Spectroscopy. *J. Phys. Chem. C* **2016,** *120*, 24382-24388.

50. Chen, D. Z.; Song, Z. X.; Chen, F.; Huang, J.; Wei, J.; Zhao, Y. X. Simply Controllable Growth of Single Crystal Plasmonic Au-Ag Nano-Spines with Anisotropic Multiple Sites for Highly Sensitive and Uniform Surface-Enhanced Raman Scattering Sensing. *RSC Adv.* **2016,** *6*, 66056-66065.

51. Hsu, K. C.; Chen, D. H. Highly Sensitive, Uniform, and Reusable Surface-Enhanced Raman Scattering Substrate with TiO_2 Interlayer between Ag Nanoparticles and Reduced Graphene Oxide. *ACS Appl. Mater. Interfaces* **2015,** *7*, 27571-27579.

52. Liu, J.; Meng, G. W.; Li, Z. B.; Huang, Z. L.; Li, X. D. Ag-NP@Ge-nanotaper/Si-Micropillar Ordered Arrays as Ultrasensitive and Uniform Surface Enhanced Raman Scattering Substrates. *Nanoscale* **2015,** *7*, 18218-18224.

53. Liu, X.; Shao, Y.; Tang, Y.; Yao, K. F. Highly Uniform and Reproducible Surface Enhanced Raman Scattering on Air-stable Metallic Glassy Nanowire Array. *Sci. Rep.* **2014,** *4*, 5835.

54. Liu, Z.; Yang, Z. B.; Peng, B.; Cao, C.; Zhang, C.; You, H. J.; Xiong, Q. H.; Li, Z. Y.; Fang, J. X. Highly Sensitive, Uniform, and Reproducible Surface-Enhanced Raman Spectroscopy from Hollow Au-Ag Alloy Nanourchins. *Adv. Mater.* **2014,** *26*, 2431-2439.

55. Wang, X.; Li, M. H.; Meng, L. Y.; Lin, K. Q.; Feng, J. M.; Huang, T. X.; Yang, Z. L.; Ren, B. Probing the Location of Hot Spots by Surface-Enhanced Raman Spectroscopy: Toward Uniform Substrates. *ACS Nano* **2014,** *8*, 528-536.

56. Li, D. W.; Pan, L. J.; Li, S.; Liu, K.; Wu, S. F.; Peng, W. Controlled Preparation of Uniform TiO_2-Catalyzed Silver Nanoparticle Films for Surface-Enhanced Raman Scattering. *J. Phys. Chem. C* **2013,** *117*, 6861-6871.

57. Chen, H. P. M.; Pang, L.; King, A.; Hwang, G. M.; Fainman, Y. Plasmonic Coupled Nanotorch Structures Leading to Uniform Surface Enhanced Raman Scattering Detection. *Nanoscale* **2012,** *4*, 7664-7669.

58. Li, W. D.; Ding, F.; Hu, J.; Chou, S. Y. Three-Dimensional Cavity Nanoantenna Coupled Plasmonic Nanodots for Ultrahigh and Uniform Surface-Enhanced Raman Scattering Over Large Area. *Opt. Express* **2011,** *19*, 3925-3936.

59. Greene, L. E.; Law, M.; Tan, D. H.; Montano, M.; Goldberger, J.; Somorjai, G.; Yang, P. D. General Route to Vertical ZnO Nanowire Arrays Using Textured ZnO Seeds. *Nano Lett.* **2005,** *5*, 1231-1236.

60. Taflove, A.; Hagness, S. C. Electrodynamics Entering the 21st Century. In *Computational electrodynamics: the finite-difference time-domain method*; Artech House: Boston, 2000; pp 1-34.

61. Palik, E. D. Comments on the Optical Constants of Metals and an Introduction to the Data for Several Metals. In *Handbook of optical constants of solids*; Lynch, D. W., Hunter, W. R., Eds.; Academic Press: San Diego, 1998; pp 275-367.

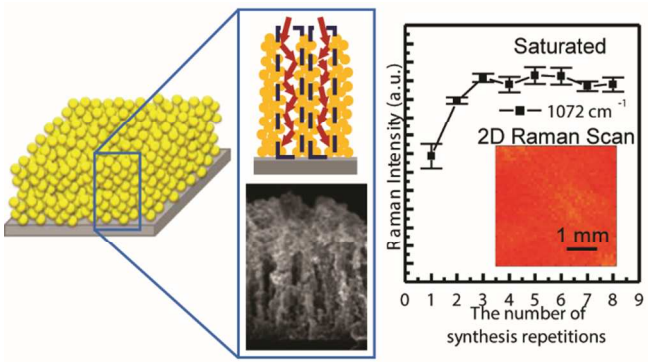

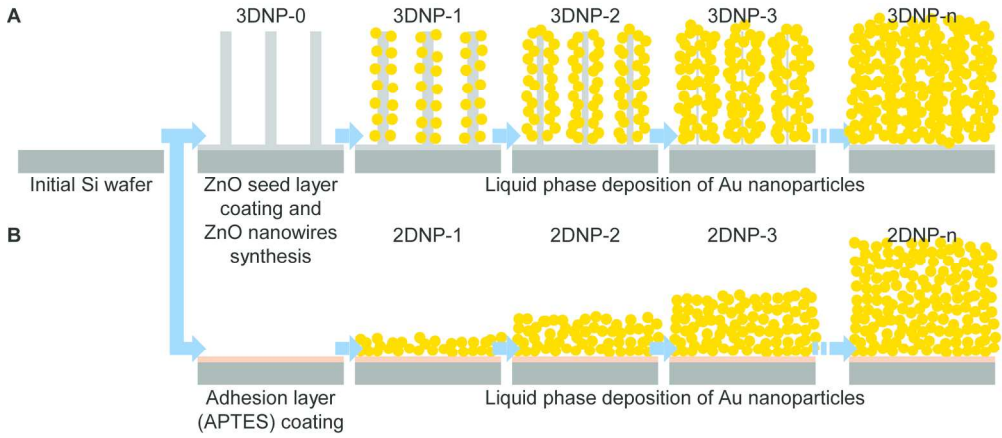

Figure 1. A schematic of the fabrication process for (A) 3D-stacked gold-nanoparticle clusters built on a Si wafer using ZnO nanowires (3DNP samples) and (B) gold-nanoparticle coated Si wafer (2DNP samples).

178x77mm (300 x 300 DPI)

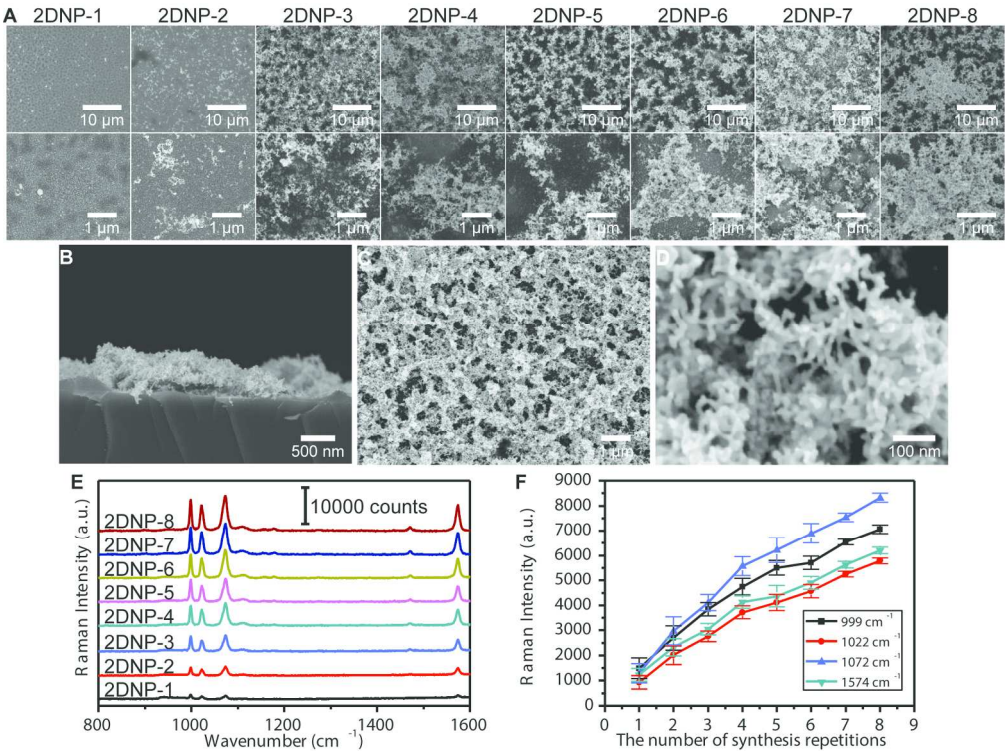

Figure 2. SEM images of (A) the top view of the gold nanoparticle film coated substrates (2DNP substrates) with varying AuNP LPD repetitions (1-8); (B) the cross sectional view and (C, D) top views of 2DNP-8; (E) SERS spectra of 2DNP-1 through 2DNP-8 1 mM benzenethiol solutions and (F) the Raman intensities at wavenumbers of 999, 1022, 1072 and 1574 cm^{-1} measured on the 2DNP substrates as a function of synthesis repetitions.

178x133mm (300 x 300 DPI)

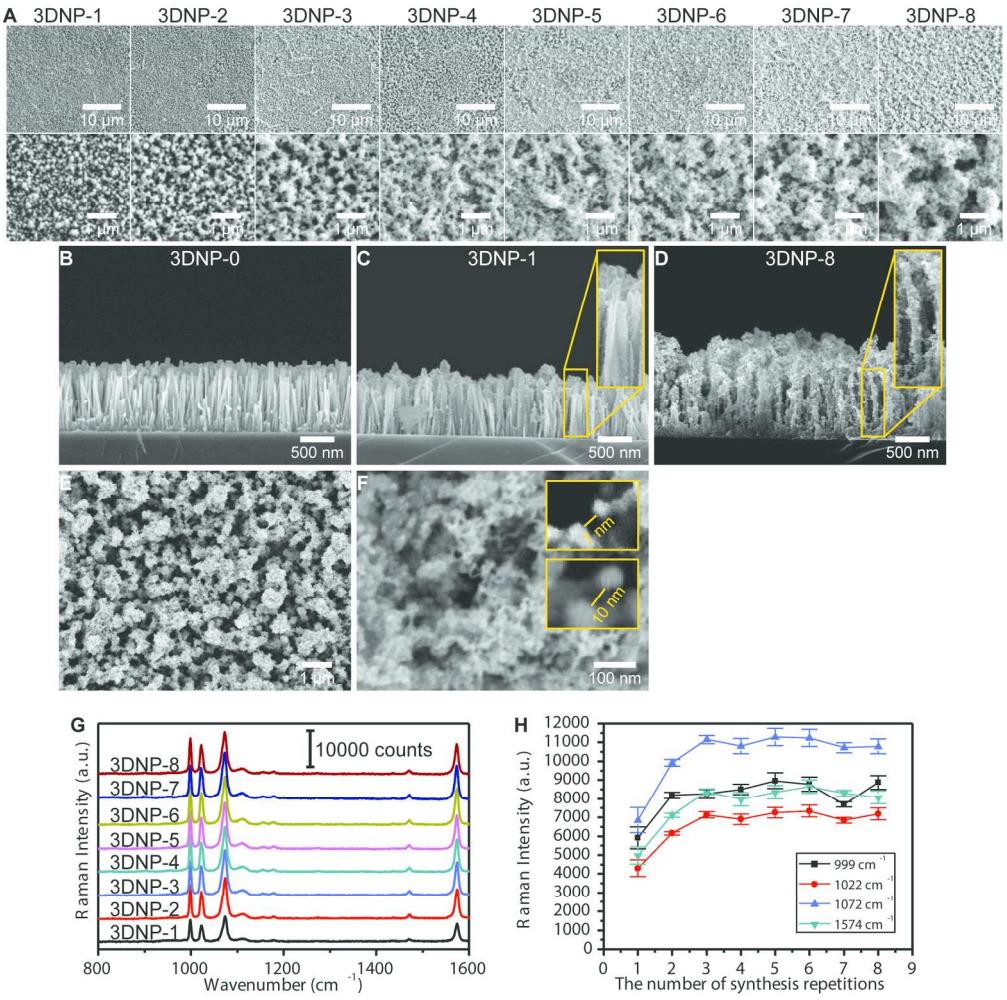

Figure 3. Top view SEM images of 3DNP substrates, which were made of ZnO nanowires grown on a Si wafer substrate and repetitive AuNP LPD processes (3DNP substrates); (B-D) cross sectional views of the ZnO nanowires before gold nanoparticle deposition (3DNP-0) and after Au NPs deposition (3DNP-1 and 3DNP-8); (E,F) top views of the of the 3DNP-8 sample; (G) SERS spectra of 1 mM benzenethiol solution and (H) Raman intensities at 999, 1022, 1072 and 1574 cm^{-1} measured on 3DNP substrates with variation in LPD repetitions.

178x176mm (300 x 300 DPI)

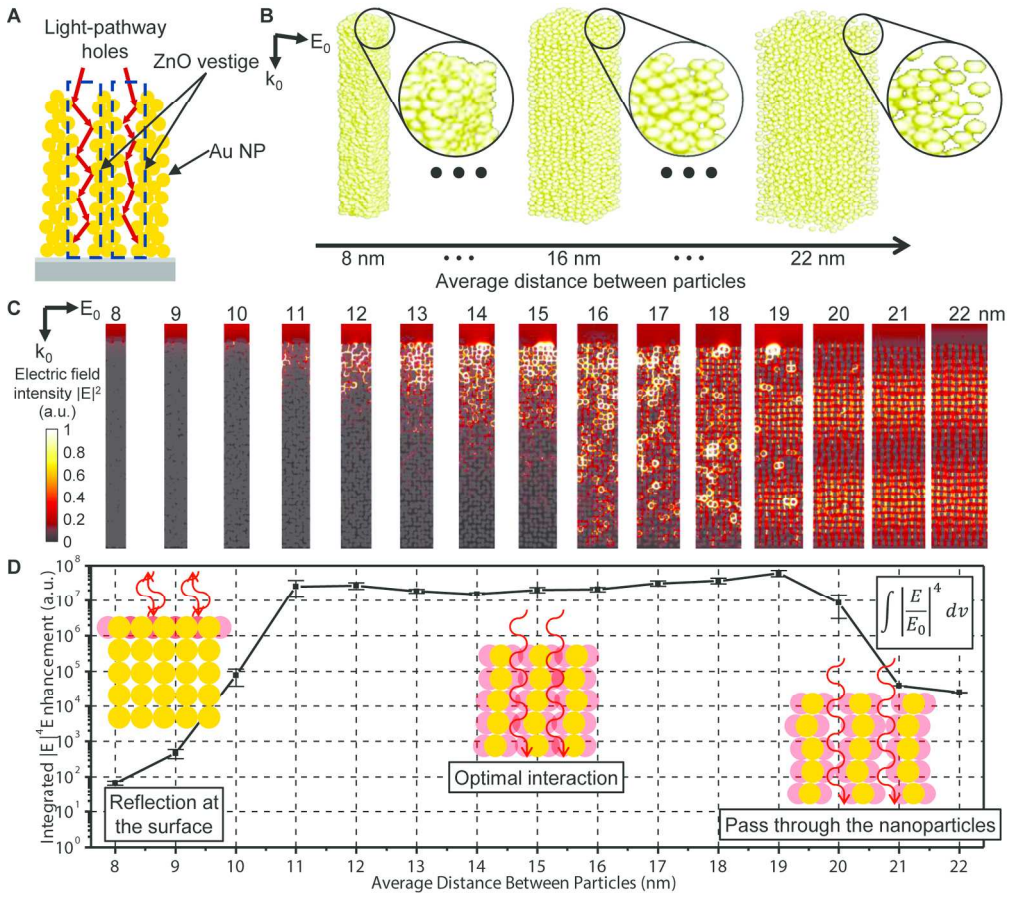

Figure 4. (A) A schematic illustration of the nanoparticle clusters with light-passing perforations of the 3DNP substrates; (B) geometry of 3DNP substrate for numerical simulation; (C) numerical simulation results of electric field intensity ($|E|^2$) distribution with various gap sizes and (D) the relationship between integrated $|E|^4$ enhancement and the particle-to-particle gap size.

178x158mm (300 x 300 DPI)

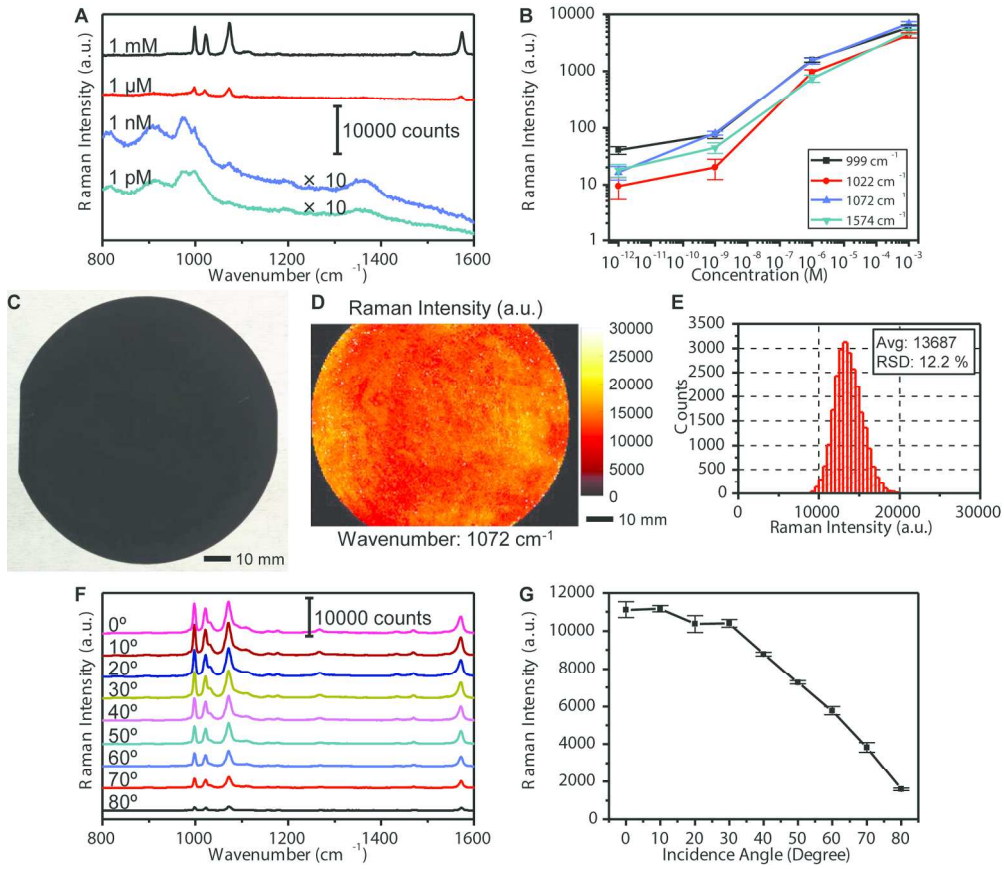

Figure 5. (A) SERS spectra of 1 mM, 1 μM, 1 nM and 1 pM benzenethiol solution and (B) the SERS intensity at 999, 1022, 1072 and 1574 cm^{-1} with various concentrations of benzenethiol solution; (C) photo of 3D stacked AuNPs synthesized on 4 inch Si wafer; (D) 2D mapping and (E) intensity distribution of 1072 cm^{-1} peak of 1 mM benzenethiol incubated 3D stacked AuNP synthesized on 4 inch Si wafer; (F) SERS spectra of 1 mM benzenethiol incubated 3D stacked AuNP substrate with various incidence angles and (G) the relationship between SERS intensity and incidence angle.

178x153mm (300 x 300 DPI)

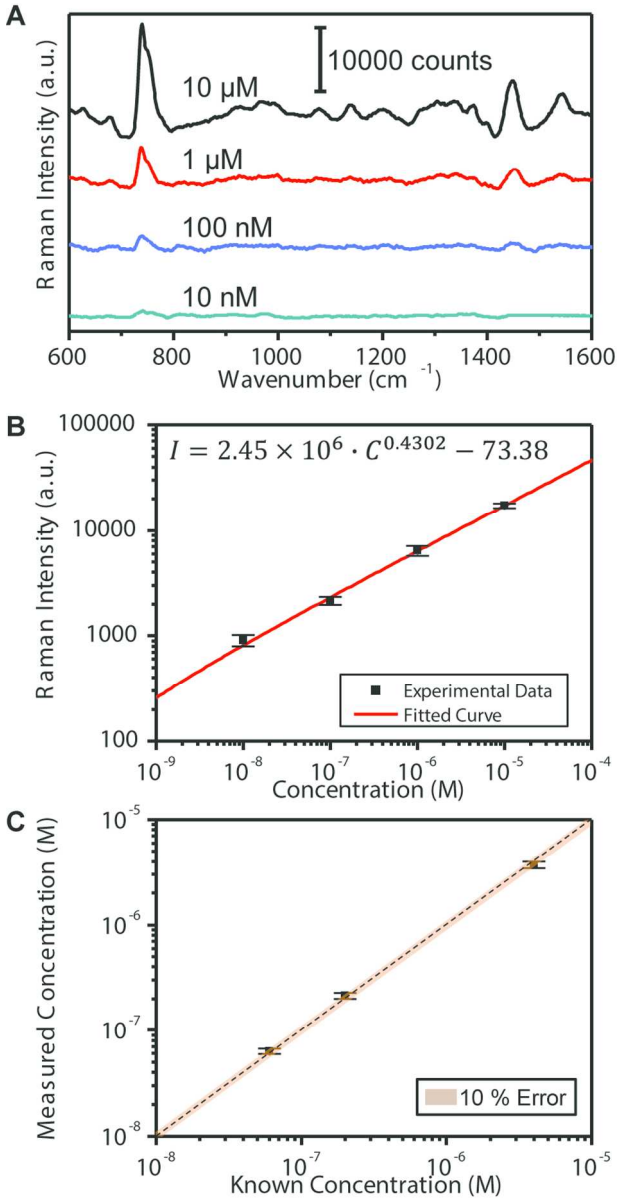

Figure 6. (A) Reference SERS spectra of 10 μM, 1 μM, 100 nM and 10 nM adenine solutions measured using 3DNP-8; (B) the experimentally measured reference relationship between the concentration of adenine solution and SERS intensity; (C) concentration readouts for adenine solutions using 3DNP-8.

78x152mm (300 x 300 DPI)